

Bernhard C. Meyer
Olaf Peter
Markus Nagel
Martin Hoheisel
Bernd B. Frericks
Karl-Jürgen Wolf
Frank K. Wacker

Electromagnetic field-based navigation for percutaneous punctures on C-arm CT: experimental evaluation and clinical application

Received: 31 January 2008
Accepted: 26 April 2008
© European Society of Radiology 2008

B. C. Meyer (✉) · O. Peter ·
B. B. Frericks · K.-J. Wolf ·
F. K. Wacker
Department of Radiology and Nuclear
Medicine, Charité - University
Hospital, Campus Benjamin Franklin,
Hindenburgdamm 30,
12200 Berlin, Germany
e-mail: Bernhard.Meyer@charite.de
Tel.: +49-30-84453041
Fax: +49-30-84454474

M. Nagel
CAS innovations AG,
Heusteg 47,
91056 Erlangen, Germany

M. Hoheisel
Siemens Healthcare,
Siemensstr. 1,
91301 Forchheim, Germany

F. K. Wacker
Radiology Department, Division of
Vascular and Interventional Radiology,
The Johns Hopkins Hospital,
Baltimore, MD 21287-0851, USA

Abstract The aim of this study was to prospectively evaluate the needle visualization and placement error and use of an electromagnetic field-based tracking navigation device for puncture procedures based on C-arm CT (CACT) images. A commercially available navigation device was mounted on an angiographic X-ray system setup for CACT. After the target was defined, needle placement was performed under real-time visualization of the virtual needle in CACT images. The final, real needle position was assessed by CACT. Punctures were performed in phantoms ($n=76$) and in twelve patients (eight biopsies, three drainages, one injection). Procedure times, system error, user error and total error were assessed. In phantoms, mean total error was 2.3 ± 0.9 mm, user error was 1.4 ± 0.8 mm and system error was 1.7 ± 0.8 mm. In the patient study, the targeted puncture was successful in all twelve cases. The mean total error was

$5.4\text{ mm}\pm 1.9$ mm (maximum 8.1 mm), user error was 3.7 ± 1.7 mm, system error was 3.2 ± 1.4 mm and mean skin-to-target time was less than 1 min. The navigation device relying on CACT was accurate in terms of needle visualization and useful for needle placement under both experimental and clinical conditions. For more complex procedures, electromagnetic field-based tracking guidance might be of help in facilitating the puncture and reducing both the puncture risk and procedure time.

Keywords Percutaneous puncture · Imaging guidance · Navigation · C-arm CT

Abbreviations EMT: electromagnetic field-based tracking · ND: navigation device · CACT: C-arm computed tomography · FOV: field of view · MPR: multiplanar reformatted images · T: target · VN: virtual needle · RN: real needle

Introduction

Percutaneous punctures under CT guidance have traditionally relied on intermittent CT images or on CT fluoroscopy which allows continuous monitoring of the needle position [1–3]. Intermittent control CT images facilitate a stepwise control of the actual needle position during the puncture without online guidance. In compli-

cated cases this can result in long procedure times [3]. The use of continuous CT fluoroscopy with continuous low dose CT allows one to view the biopsy needle as it is advanced in real time. This leads to a significantly lower needle placement time for CT fluoroscopy compared with that of intermittent CT control techniques [1, 3]. However, it also leads to a significant increase in radiation exposure [3].

To overcome radiation exposure, electromagnetic field-based tracking (EMT) can be used. Navigation systems provide navigation information visualizing the tip of the interventional device (e.g. puncture needle, probe or guide wire) as well as roadmap information obtained by using CT images acquired directly before the procedure [4]. Careful trajectory planning within the 3D CT roadmap allows the physician to see nearby anatomy without additional radiation exposure. Such systems are utilized for neurosurgical procedures [5]. On CT, most procedures are performed without navigation systems; however, with the advent of C-arm cone-beam computed tomography (CACT) or angiographic computed tomography, navigation systems have received increased interest. CACT is a relatively new technique that uses data acquired with a flat-panel detector C-arm angiography system to reconstruct cross-sectional, CT-like images. CACT allows a contrast resolution of 10 HU as well as a slice thickness and in-plane resolution of less than 1 mm. Unlike conventional multidetector computed tomography (MDCT), the tube detector system in CACT is not mounted within a gantry, allowing free access to the patient immediately after imaging without moving the patient. This makes CACT an ideal tool for percutaneous punctures. In addition, the field generator required for EMT can easily be placed near the patient. CACT is favourably supplemented by such a navigation system because the current systems lack an inbuilt laser sight. When a percutaneous puncture has to be performed under CACT guidance without the use of a navigation tool, finding the entry point on the skin in relation to the deeper laying target is much more difficult with CACT than with MDCT.

The purpose of this study is to evaluate the accuracy of needle visualization of an EMT system in combination with a CACT and the needle placement error using the system as a navigation tool for percutaneous punctures in both phantoms and patients.

Materials and methods

Navigation hardware and procedure

The EMT system requires three steps to facilitate exact needle tracking. First, CACT images are acquired with a fixed reference frame inside the region to be examined. The reference frame consists of five radio-opaque markers and a detector comprised of two sensor coils with a definite distance and location to each other. After data acquisition and image reconstruction, the 3D data set is sent to the navigation system.

The second step is registration of the imaging space with the electromagnetic needle guide space using the reference frame. An electromagnetic field generator (Aurora; Northern Digital, Waterloo, ON, Canada) is placed in proximity to the phantom or to the patient. The field generator

produces an ultra-low electromagnetic field. As a very weak current that is dependent on the position and orientation of the detector is induced in the sensor coils of the reference, it can be localized within the electromagnetic space. Co-registration of the imaging space and the electromagnetic space is automatically performed by the navigation system which detects the radio-opaque markers embedded in the reference frame in the imaging space and then locates the position of the reference frame detector in the electromagnetic space (Fig. 1).

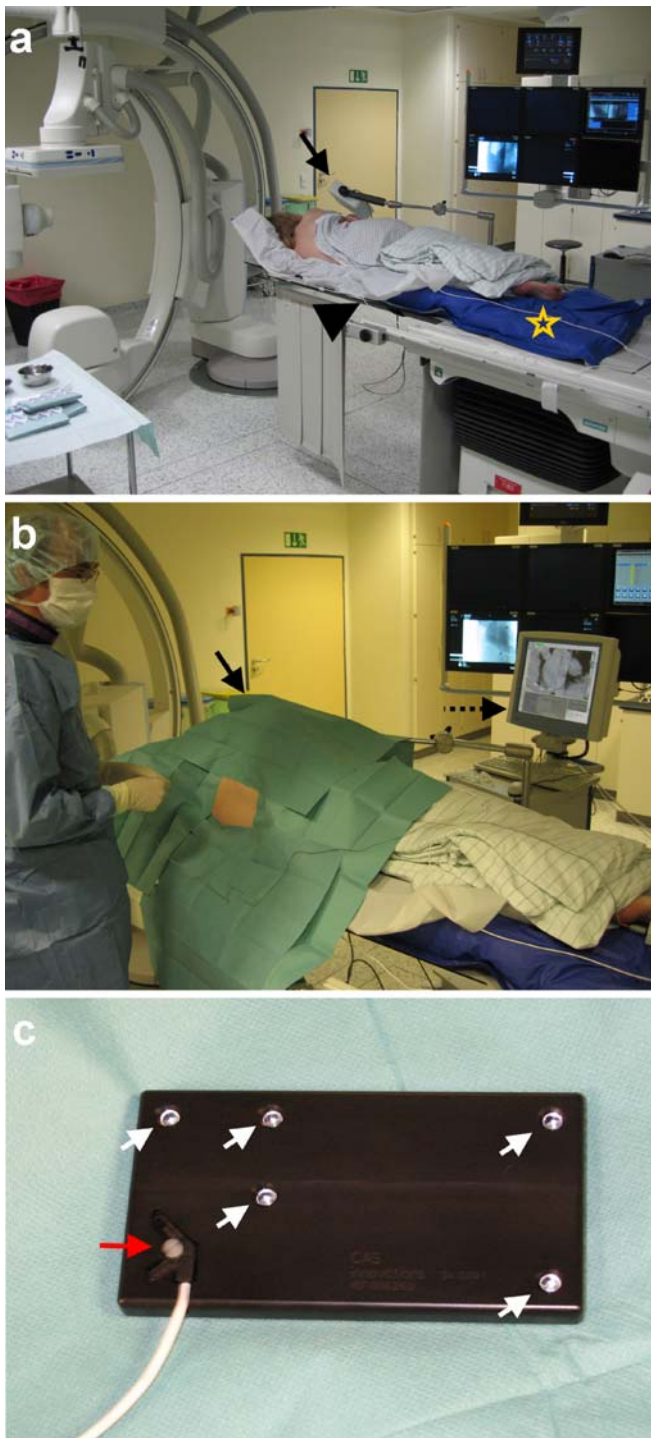
The third step is the actual needle tracking. An 18-G needle (Amedo GmbH, Bochum, Germany) with coils integrated in the tip was used. A wire connects the needle to the navigation system (Aurora control box; NDI, Ontario, Canada). As the current induced in the coil is dependent on the orientation and position of the needle, the interface is able to compute and to convey the position of the needle tip to the navigation system (CAPPA IRAD EMT; CAS innovations AG, Erlangen, Germany). This enables both real-time tracking of the needle in the electromagnetic space and display of the needle position within the co-registered imaging space during manipulation [6].

CACT imaging technique

CACT images of the phantoms and patients were acquired with an angiography flat detector C-arm (Axiom-Artis dBA VB31C; Siemens Healthcare, Forchheim, Germany) using the 8sDR preset (DynaCT[®]; Siemens Healthcare, Forchheim, Germany) with an acquisition time of 8 s, a total projection angle of 240°, projection increment 0.5°, 1-k matrix, zoom factor 0, field of view 480 mm and a system dose per pulse of 0.36 μ Gy. With the detector used, the volume covered had a cylindrical shape with a height of 185 mm (craniocaudal coverage), a diameter of 225 mm (transverse and sagittal range) and a voxel size of 0.4 mm. All patient CACT examinations were performed without breath-hold. The time from the end of the data acquisition to the presentation of cross-sectional images on the reconstruction workstation (syngo X Workplace, VA72A; Siemens Healthcare, Forchheim, Germany) ranged from 43 to 45 s.

Spike phantom

To estimate the technical error of the navigation device, a phantom consisting of 11 Plexiglas[®] spikes was examined. After positioning of the field generator and automatic registration of the imaging space with the electromagnetic space, the spike tips were defined as targets. An EM traceable core needle was adjusted on the spike. The distance of the virtual needle tip from the target was measured in three dimensions by the navigation device,



◀ **Fig. 1** Setting of the navigation device. Overview (a) and close-up (b) of the setting of the electromagnetic field-based navigation device (ND). The patient is bedded on a vacuum mattress (*asterisk*). The field generator (*black arrow*) is attached to the patient table and connected to the ND (*dotted arrow* in b). c Photograph of the reference frame with two embedded sensor coils (*red arrow*) and five radio-opaque markers (*white arrows*), which is fixed underneath the patient (position shown in a, *arrowhead*) and included in the CACT volume. Due to the definite spatial relation of the markers and the sensor coils, co-registration of the imaging space and the electromagnetic space is performed automatically by the ND which detects the radio-opaque markers in the imaging space and locates the position of the sensor coils in the reference frame detector in the electromagnetic space

Puncture phantom

The biopsy phantoms consisted of square buckets filled with nontransparent candle gel wax. To mimic lesions within the phantom, 19 plastic rings, each with an inner diameter of 7 mm and a height of 1 mm, were embedded in the gel phantom. The rings were placed, each with its longitudinal axis parallel to that of the bucket, at different spatial locations and levels inside the bucket. After image acquisition and registration, targets were defined in the centre of the rings. During the puncture procedure, the orientation and position of the needle tip were visualized in real time on the multiplanar reformatted images (MPR). For additional puncture guidance, a schematic tool was used to visualize the distance to the target and the consistency of the needle trajectory with those of the entry and the target point (Fig. 2b) in real time. A 20-cm-long, 18-gauge hollow needle with a retractable EM traceable core needle was used for the punctures. When the target was reached, the duration (i.e. time from displaying the target on the navigation device (ND) to reaching the final needle position) and the absolute time were recorded. The position was marked using a 4-mm-long piece of wire which was pushed through the hollow needle using a guide wire after retraction of the core needle. After completion of the puncture procedure, phantoms were rescanned with CACT.

As the phantom was not moved during the punctures, the postprocedural images and the log file were loaded into the 3D viewer tool of the navigation device. The position of the centre of the rings (target, T) and of the visualized virtual needle tip at the end of each puncture (virtual needle position, VN) as well as the coordinates of the wire end (real needle position, RN) were recorded. Phantom punctures were performed by two radiologists. Each of the operators performed two-times 19 punctures. The sample size for the study was not calculated a priori. The number of trials was predominantly determined so as to be the most reasonable within the time and resource budget restrictions.

Three different errors were calculated. The *user error* (or virtual placement error, $\Delta VN-T$) is the error made by the physician in placing the visualized virtual needle tip

and the distance, D_{3D} , was calculated as follows: $D_{3D} = \sqrt{\Delta x^2 + \Delta y^2 + \Delta z^2}$, where Δx , Δy and Δz are the distances from needle tip to target in each dimension x , y and z , respectively. For the whole phantom, the measurements were performed ten times and mean values were calculated.

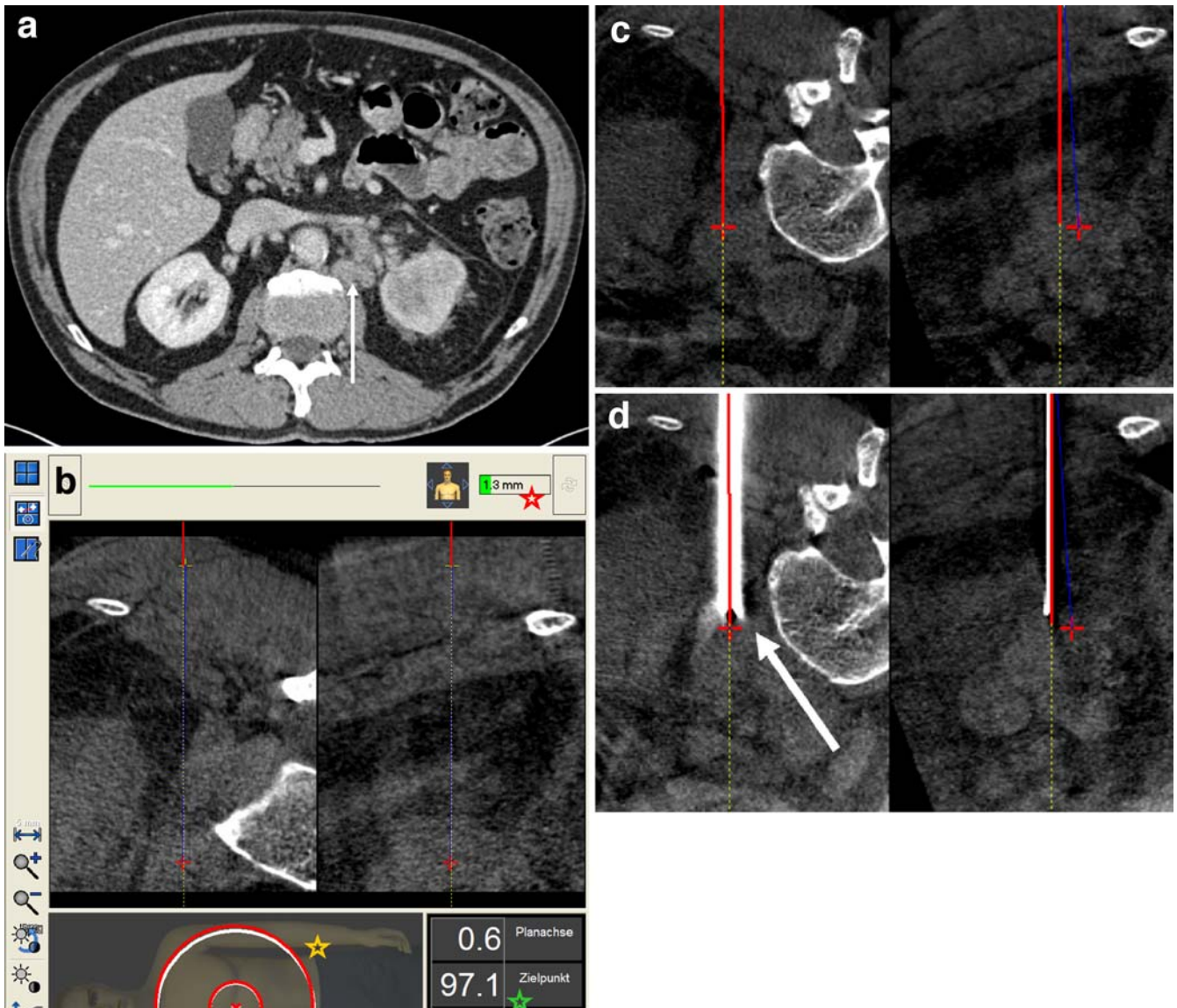


Fig. 2 Biopsy of an enlarged retroperitoneal lymph node. **a** MPR of the upper abdomen MDCT of a 67-year-old man shows multiple incidentally detected enlarged retroperitoneal lymph nodes (*arrow*). **b** Screenshot of the real-time MPR of the preprocedural CACT images orthogonal to the virtual needle (*red line*). The virtual needle extension (*yellow dotted line*) eases the correct angulation of the needle. The puncture target is indicated by the *red cross* and the planned trajectory is indicated by a *blue line*. As a schematic ring figure (*yellow asterisk*) summarizes the depth and orientation of the needle, by matching the *small white ring* (skin entry point) and the *small red ring* (virtual needle tip), the skin entry point can be

adjusted. The *large rings* represent the real (*red big ring*) and the required (*white big ring*) angulation of the needle. When both rings are matched, the needle can be advanced. The distance to the planned target is shown continuously (*green asterisk*). Patient movement is tracked and permanently visualized by a *green bar* (*red asterisk*) that turns red if the patient movement exceeds 4 mm. MPR of the preprocedural (**c**) and postprocedural (**d**) CACT image shows good correlation of the virtual needle in the final position (*red line*) with the real needle (*arrow*). Biopsy revealed a metastatic infiltration of the lymph nodes by a renal cell carcinoma

in the indicated target shown on the screen of the navigation system. This error depicts how well the physician was able to follow the guidance and depends on the quality and intuitiveness of visualization as well as of the manual skills of the physician. The user error was calculated as the distance between the virtual needle

tip recorded in the electromagnetic space at the end of the puncture in the target position and the centre of the plastic ring in all three dimensions.

The *system error* ($\Delta RN-VN$) is the distance between the final virtual needle position and the wire end in the postprocedural images (RN) in all three dimensions. This

error is comprised of the technical error of the ND and any other systematic errors such as movement of the hollow needle after retraction of the traceable core needle.

The *total error* (or real placement error, $\Delta\text{RN-T}$) is the distance from the centre of the plastic ring to the end of the wire marker position at the end of the puncture, as computed from the CACT control images. This error shows the end result which is the position of the real needle tip with respect to the centre of the lesion target and is composed of the system error and the user error.

Statistical analysis

A nonparametric repeated measures analysis of variance (Friedman test) was used to determine whether the error in a particular dimension, x , y or z , differed from the other errors. In the case of significance, post-testing was performed (i.e. Dunn's multiple comparisons test). To test for possible interactions between errors in the x , y and z dimensions, the R^2 values and the associated P values were obtained from calculations of the Pearson product-moment correlation coefficients. The R^2 value was selected for analysis to illustrate the very low proportion of variance accounted for by a linear relationship among the x , y and z error components. For all three errors, the in-plane component with the horizontal plane (in-plane distance of the two defining points; $D_{2D} = \sqrt{\Delta x^2 + \Delta z^2}$) as well as the three-dimensional (3D) distance ($D_{3D} = \sqrt{\Delta x^2 + \Delta y^2 + \Delta z^2}$) and the 95% confidence interval were calculated (Fig. 3).

To test the puncture results for a temporal learning curve, the mean of the first half of the data (D_{3D} user error, puncture time) was compared with that of the second half of the data for each operator (Mann–Whitney test). The 3D technical error estimated in the spike phantom was compared with the 3D system error from the puncture phantom using the Mann–Whitney test.

Patient study

Between June and August 2007, twelve consecutive patients (ten men, two women; mean age 67 years, age range 44–85 years) underwent CACT-guided puncture ($\Sigma=9$; direct puncture of a type-II endoleak after endovascular abdominal aortic aneurysm repair, $n=1$; histologic characterization of an osteolytic lesion in the sacrum, $n=1$; enlarged retroperitoneal lumbar or pelvic lymph nodes, $n=4$; or pleural tumours, $n=3$) or drainage ($\Sigma=3$; drainage of an abdominal abscess, $n=2$; drainage of an organizing pleural space empyema, $n=1$) using the EMT navigation system. The study was performed to validate the clinical use of the EMT system in patients. The inclusion criteria for the

study were patient willingness and ability to provide informed consent as set forth by the local ethics committee which approved the study.

Patients were placed on a vacuum mattress (BlueBAG, Bodyfix system, Medical intelligence AG, Schwabmünchen, Germany) to prevent movement during the procedure. A traceable motion sensor affixed to the patient allowed for online monitoring of relevant patient movement during the procedure. The reference board was in a fixed position between the mattress and the patient. After image acquisition and registration, the skin entry point and the target were located within the imaging volume and were interactively marked using the touch screen of the ND. After localizing the skin entry point using the puncture needle as a pointer and after adapting the entry point to the local requirements, e.g. ribs, local anesthesia was administered. In two cases, a double-angulated puncture path was chosen. The puncture procedure was performed with the needle type described in the phantom studies. Needle lengths of 5 cm, 10 cm or 20 cm were available. In the case of biopsy procedures, the outer part of the needle was used for coaxial puncture using a commercially available biopsy needle (Biopsy-Handy; Somatex Medical Technologies GmbH, Teltow, Germany) to obtain tissue samples.

During the puncture procedure, the orientation and position of the needle tip were visualized (Figs. 2 and 4), and were also logged in a file 3 times per second. Although the CACT was always on standby to acquire control CACT images during the procedure, this was not necessary in our

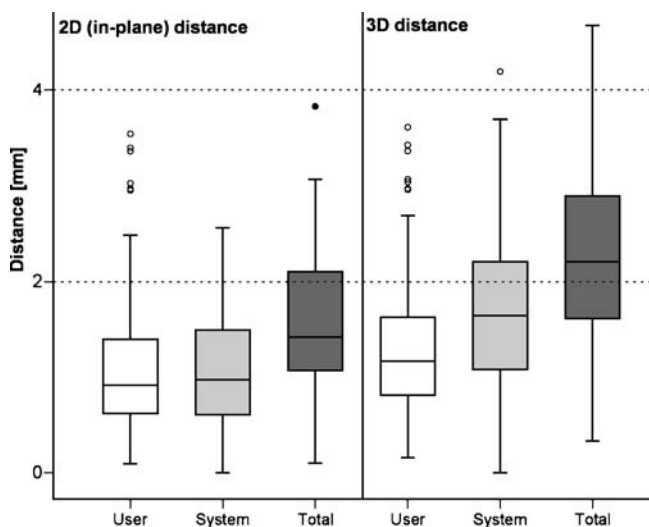


Fig. 3 Box and whiskers plot of the in-plane (2D) and 3D user error, system error and total error in the phantom study. The *box* indicates the range from the first to the third quartile, the *solid line* in the middle of the box indicates the median, *whiskers* indicate the minimum and maximum value within 1.5-fold of the box range and *circles* indicate outliers

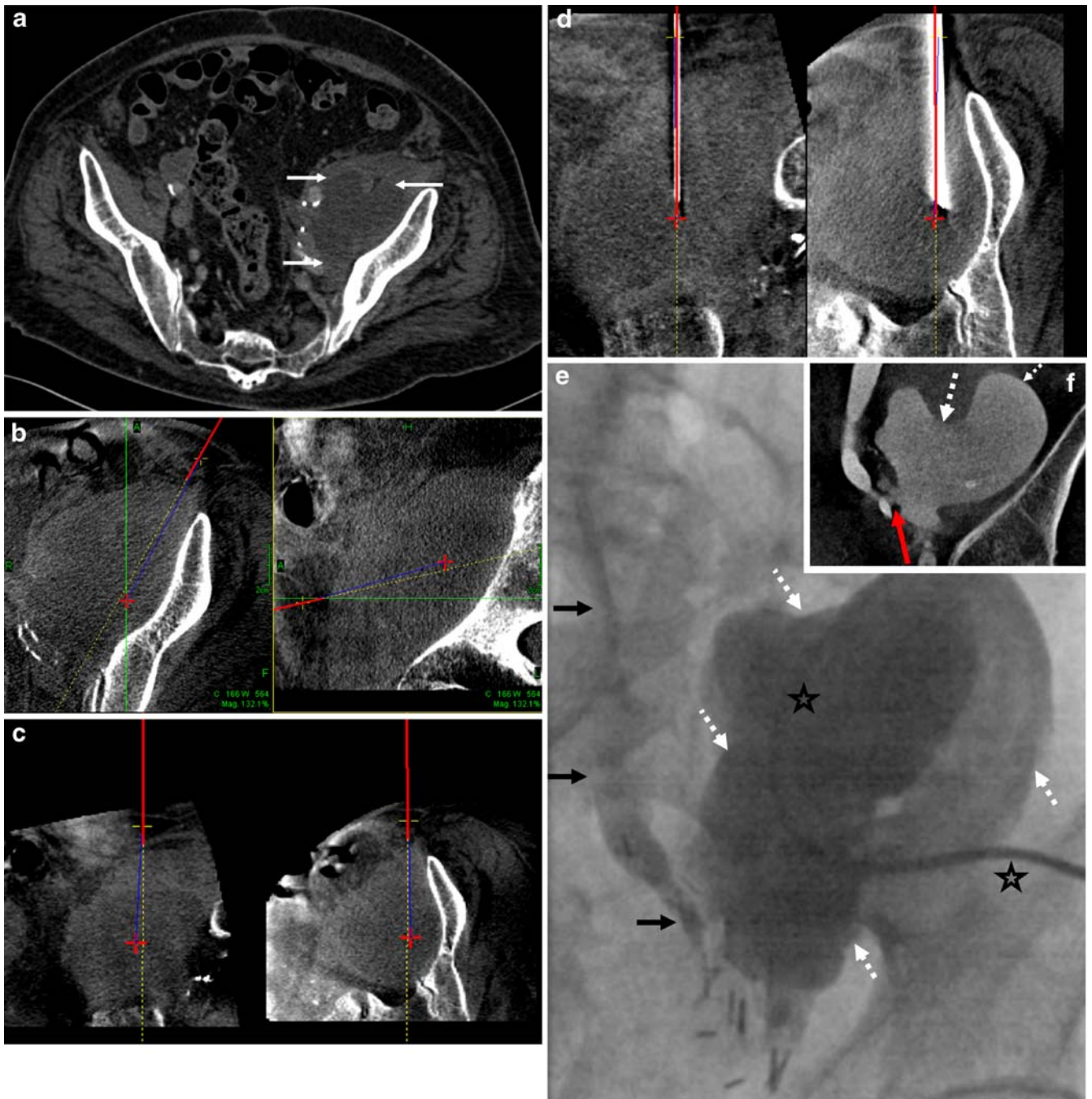


Fig. 4 Drainage of an abscess. **a** MPR of a pelvic MDCT shows a hypodense structure suspicious for being an abscess in the iliopsoas muscle (*arrows*) in an 85-year-old man after partial bladder resection due to bladder cancer. MPR of the preinterventional (**b**, **c**) and postinterventional CACT (**d**). **b** transversal and sagittal MPR show the planned trajectory (*blue line*) and selected target (*red cross*) in relation to the virtual needle position (*red line*). **c** Screenshots of the real-time MPR images of the preprocedural CACT perpendicular to the virtual needle during the needle

propagation. **d** MPR images of the postinterventional CACT perpendicular to the final virtual needle position, confirm the correct needle placement. **e** Fluoroscopy after drainage of purulent fluid over a placed pigtail catheter (*asterisk*) and contrast instillation in the drained cavity (*dotted arrows*) shows retrograde filling of the dilated ureter (*arrows*). **f** MPR of the CACT shows the insufficiency of the ureter (*red arrow*) and proves the structure to be an infected urinoma (*dotted arrows*)

cases. When the final target position was reached, a CACT image with the needle in place and the reference board included in the image volume was acquired. The postprocedural images, the log file and the preprocedural images were loaded into the 3D viewer tool of the ND and the coordinates of the target (T), the visualized virtual needle tip at the end of the puncture (VN) and the coordinates of the real needle tip (RN) were recorded. The 3D user, system and total errors were estimated according to the puncture phantom experiment.

Preprocedural imaging time (CACT raw data acquisition, transfer to the reconstruction workstation and cross-sectional image reconstruction), image transfer time (cross-sectional image transfer from the reconstruction workstation to the ND), puncture planning time (initial planning of the skin entry point and the target), total prepuncture time (time from CACT raw data acquisition to completion of the initial puncture planning), planning-to-puncture time (localizing of the skin entry point with the needle, changing and resetting of the skin entry point if necessary, and local anesthesia) and the skin-to-target time and mean duration (time from CACT raw data acquisition to confirmation of needle position on postprocedural images) were documented for every procedure.

Results

Spike phantom

Measurement of the technical error in the spike phantom showed a mean deviation of $1.0 \text{ mm} \pm 0.3$ (standard deviation) with a maximum error of 1.9 mm. This error represents the accuracy of the navigation device and reflects the registration error of the electromagnetic and the imaging spaces.

Puncture phantom

Using EM guidance, the interventionalist was able to locate an appropriate point of entry into the phantom by matching the two large rings in the schematic orientation figure on the ND monitor. Needle angulation and the distance of the needle tip to the target during the puncture were intuitively visualized. The physicians were able to insert the needle with a firm and constant motion along the desired straight needle path all the way to the target. The mean puncture time from the display of the targets on the ND monitor to the final needle position was 36 s (range 14–93 s). There was no significant difference in mean puncture time between the first and the second half of the punctures for either operator (operator 1 $P=0.64$, operator 2 $P=0.063$).

There was no significant difference in the errors in the x , y and z dimensions for the user error ($P=0.41$). The mean system error in the y dimension (depth) was slightly but

significantly higher than that in the x and z dimensions ($\Delta y=1.2 \pm 0.8 \text{ mm}$ vs. $\Delta x=0.7 \pm 0.6 \text{ mm}$, $P<0.001$; $\Delta z=0.6 \pm 0.5 \text{ mm}$, $P<0.001$) as was the mean total error in the y dimension compared with that in the z dimension ($\Delta y=1.4 \pm 1.0 \text{ mm}$ vs. $\Delta z=0.8 \pm 0.7 \text{ mm}$, $P<0.01$). There was no correlation between the errors in x , y and z dimensions for all three calculated errors. R^2 values ranged from 0.001 (user error, Δz vs. Δy) to 0.072 (total error, Δy vs. Δx).

In all 76 punctures, the radiologists correctly placed the tip of the needle inside the lesion targets. As recorded on the CACT images of the phantom after the puncture, all marker wires were inside the 7-mm-diameter ring in the transverse plane.

The mean in-plane (2D) user error was $1.2 \pm 0.8 \text{ mm}$ with a maximum error of 3.5 mm, and the mean 3D user error was $1.4 \pm 0.8 \text{ mm}$ with a maximum error of 3.6 mm (Fig. 3).

This result represents the precision with which the radiologist is able to perform the ND-guided needle placement procedure, assuming that the ND system itself is error-free. Six outliers were observed in both groups. Over both operators, five outliers were observed in the first half of the punctures, while only one outlier was in the second half. This might reflect a mild learning curve. Nevertheless, despite a slight decrease in mean 3D user error between the first and the second half of the punctures for both operators (operator 1, $1.8 \pm 0.8 \text{ mm}$ vs. $1.4 \pm 0.8 \text{ mm}$; operator 2, $1.1 \pm 1.0 \text{ mm}$ vs. $1.0 \pm 0.7 \text{ mm}$), there was no significant difference between the two groups for either operator (operator 1 $P=0.08$, operator 2 $P=0.58$).

The mean in-plane system error was $1.1 \pm 0.6 \text{ mm}$ with a maximum error of 2.5 mm. The mean 3D system error was $1.7 \pm 0.8 \text{ mm}$ with a maximum error of 4.1 mm which was significantly higher compared with the sole technical error shown by the spike phantom ($n=220$, $1.0 \pm 0.3 \text{ mm}$, $P<0.0001$).

The mean in-plane (2D) total error was $1.6 \pm 0.8 \text{ mm}$ with a maximum error of 3.8 mm, and the mean 3D total error was $2.3 \pm 0.9 \text{ mm}$ with a maximum error of 4.7 mm.

Patient puncture

Visualization of the virtual needle in the perpendicular real-time MPR in relation to the indicated target (Figs. 2 and 4) provided abundant information and guidance, leading to a straightforward puncture with an average skin-to-target time of 49 s (range 15–120 s) albeit with a single or double angulation of the puncture path. Preprocedure imaging took less than 2 min in all patients, and the mean image transfer time to the ND was less than 1 min. The average mean duration was 15 min 38 s. All procedure times are shown in Table 1.

The targeted puncture was successful in all twelve cases (in view of having obtained histological representative material, puncturing the endoleak sac or aspiration of pus),

Table 1 Procedure time in the patient study

Parameter	Mean time (range) (min:s)
Preprocedure imaging time	1:28 (1:28–1:30)
Image transfer time	0:39 (0:16–2:14)
Planning time	1:49 (0:11–5:21)
Total prepuncture time	8:47 (3:51–16:21)
Planning-to-puncture time	3:51 (0:57–11:21)
Skin-to-target time	0:49 (0:15–2:00)
Duration (from the initial to the final control CACT)	15:38 (22:40–32:12)

with a maximum error of 7 mm in a particular dimension, x , y or z . The mean Pythagorean distance from the puncture needle to the target (3D total error) was 5.4 mm (standard deviation 1.9 mm) with a maximum of 8.1 mm. The 3D user error was 3.7 mm (standard deviation 1.7 mm), and the 3D system error was 3.2 mm (standard deviation 1.4 mm). The maximum patient motion recorded by the motion sensor was 5 mm.

Discussion

The EMT device presented in this study has been proven to effectively facilitate needle navigation based on CACT images. The ND system uses CACT images acquired immediately before the procedure and co-registers them with the electromagnetic space, thus providing real-time visualization of the tracked needle in MPR images of the CACT. MPR images are reconstructed transversal and sagittal to the patient axis as well as orthogonal to the needle path. The combination of the MPR views and the ring figure makes hand-eye coordination very intuitive. By simply matching the two small rings, the entry point can easily be located. If the entry point needs to be changed for anatomical reasons, the tip of the needle must be adjusted and a single mouse click resets the entry point to this position. Correct angulation of the needle is obtained by matching the two big rings. Propagation of the needle is monitored and the distance to the planned target is calculated in order to obtain correct needle depth positioning.

Reflecting this intuitive handling, a 3D user error in the patient study of 3.7 mm (standard deviation 1.7 mm) and a 3D total error of 5.4 mm (standard deviation 1.9 mm) could be achieved and the mean skin-to-target time was less than 1 min, which is well tolerable in a clinical setting for most targets. We observed a slight, statistically not significant decrease of the user error between the first and the second half of the punctures for both operators, which might reflect a mild learning effect, as five of six outliers were observed in the first half of the punctures and only one in the second half. Considering the low user error, this proves that the

visualization is intuitive and easy to anticipate for the interventional radiologist.

The 3D system error of 3.2 mm (standard deviation 1.4 mm) in the patient punctures was slightly higher compared with the technical error estimated in the puncture phantom of 1.7 mm (standard deviation 0.8 mm) and in the spike phantom of 1.0 mm (standard deviation 0.3 mm). This is probably due to the fact that the system error in the patient study comprises the technical error as well as any other deviations caused by movements of the needle between control acquisition and placement. The slightly higher mean system error in the depth dimension compared with the x and z dimensions in the phantom study is most likely caused by the properties of the gel wax used for the puncture phantoms. When the wire piece was inserted over the hollow needle and the wire pusher was drawn back, the wire piece was probably pushed back because of the elasticity of the gel wax or it might have been drawn back in the puncture tract due to a vacuum phenomenon. Nevertheless, for the intended use of the system for biopsy and drainage, this range of the technical error as well as that of the total error achieved is undoubtedly acceptable. A recent study by Krücker et al. evaluated the technical error (or tracking error) of a very similar electromagnetic tracking device used in 19 patients undergoing US-guided punctures on a CT table [7], but the operator was blinded to the tracking display. The slightly higher tracking error (corresponding to the technical error in our study) of 5.8 ± 2.6 mm in this study showed a weak negative correlation between the tracking error and the distance from the CT table, suggesting that a large portion of the basic tracking error in this study can be explained by field distortions introduced by the CT system [7]. By comparison, the carbon fiber patient table and the C-arm did not cause relevant field distortions as shown in our spike phantom experiment. Nevertheless liability for field distortions are a potential weakness of any EMT system if metal is close to the operation field. The system used in our study avoids inaccurate needle tracking by tracking field homogeneity. The main advantage of the current system over optical navigation systems is that the actual needle tip is tracked,

whereas in other systems, the tip must be calculated from the position and orientation of the needle end outside the body. Therefore, known limitations such as line-of-sight problems with the optical markers at the needle end and positioning errors due to needle bending have been overcome in the current system.

In comparison with MR- or MDCT-guided punctures, the gantry diameter and needle length are not limiting factors because the actual procedure is performed without any spatial restrictions as the angiography table can be freely moved prior to and during the procedure. With this setting, fluoroscopic control is always available if needed and can be used to control an intracavitary needle position by contrast injection or to place drainage catheters. This has been shown to significantly reduce the procedure times with drainage catheter revisions and postinterventional drainage periods [8]. In comparison with most CT units, the angio room is better suited for interventional procedures as the staff are well trained to handle interventional equipment and patients, and sterility is easier to achieve than in a usually busy CT unit with its high patient throughput.

A different approach for needle guidance based on CACT images recently developed and presented by Racadio et al. [9] is to visualize the target and puncture path in fluoroscopic images based on 3D information of an CACT. The main advantage of this approach over EMT is that this method gets by without additional devices, such as navigation terminals and dedicated needles. On the other hand, it needs intermittent fluoroscopic controls and provides no real-time monitoring of the needle position and a needle-holding device has to be used to avoid radiation exposure to the hand of the physician.

One limitation of our study is that the flat detector (FD) angiography system used in this study has a field of view of 225 mm × 225 mm × 185 mm. As the reference board must be included in the conic CACT volume, the exact positioning of the patient and the reference board within the covered volume can be challenging. However, this shortcoming can be overcome by increasing the CACT range and the size of the FD [10] or by using a more compact reference board. The slightly lower contrast resolution of the CACT compared with that of MDCT [11] is not an issue as the initial diagnosis is usually made based on contrast-enhanced MR or CT images. Based on these findings, the CACT facilitated the localization of the target lesions in all of our patients.

Another limitation of the setup is that the patient must be immobilized during the intervention. Deflation of the vacuum mattress added 20 s to the preprocedure setup. The motion sensor allowed for detection of patient movement during the puncture. Internal organ movement is another challenge which restricts use of the current system to targeting retroperitoneal, musculoskeletal, pelvic and pleural lesions without relevant movement caused by breathing. To target liver lesions, a breathing motion correction must

be implemented. There are simple solutions which have already been implemented for CT-guided punctures [12]. More complex solutions could be based on methods used in radiation therapy as well as on those used in positron emission tomography–CT image fusion [13–17]. However, neither patient nor breathing motion correction will account for the internal target displacement or deformation which can occur during needle advancement. This can be overcome by performing control imaging during the course of an intervention, similar to that which is normally done with CT guidance or, technically more challenging, by using a deformable finite element model that predicts deformations of the target organ [18, 19].

Until recently, the use of EMT was reported for navigation during transjugular intrahepatic portosystemic shunt creation, vena cava filter placement, cardiac catheterization, bone screw deployment, liver biopsy, venous catheter placement, and bronchoscopy [20–23], but the use of these systems was limited to phantoms or animals. In patients, an electromagnetic tracking system that uses the images of the video output of a CT scanner has been evaluated by Holzkecht [12]. A limiting factor with this system was that the tracking sensor had to be fixed at the bottom of the needle due to size restrictions. Therefore, needle bending could not be detected or taken into account when advancing the needle. Despite this shortcoming, the reported technical error using this system was 2.2 mm. However, this system is not commercially available. A more recent study evaluated the feasibility of using preprocedural imaging for guide wire, catheter and needle navigation in phantoms and in a swine model. The study was able to show that the use of EMT devices within previously acquired imaging datasets allows for a precise visualization with reconstructed imaging based on the position and orientation of the catheters, guide wires or needles, therefore allowing a road-mapping suited to guiding an intervention with an error less than 5 mm; however, this study was also restricted to phantoms and animal models [4].

In conclusion, EMT based on CACT images for percutaneous biopsies and drainages is feasible and allows intuitive and accurate needle localization in phantoms as well as in patients. It remains to be seen what procedures will benefit most from this system. For simple procedures with a straight needle path, an experienced interventionalist does not require a guidance tool, although EMT with real-time visualization of important landmarks and critical structures might be helpful for less-experienced users. However, given the cost and availability, in the foreseeable future, US and CT guidance will remain the “workhorses” for biopsy procedures.

For more complex procedures, such as double-oblique puncture trajectories or thermal tumour ablations that require positioning of multiple applicators and punctures of multiple lesions, EMT guidance might be of help to facilitate the puncture and to reduce puncture risk and procedure time even for experienced users.

References

1. Gianfelice D, Lepanto L, Perreault P, Chartrand-Lefebvre C, Milette PC (2000) Value of CT fluoroscopy for percutaneous biopsy procedures. *J Vasc Interv Radiol* 11:879–884
2. Mueller PR, vanSonnenberg E (1990) Interventional radiology in the chest and abdomen. *N Engl J Med* 322:1364–1374
3. Silverman SG, Tuncali K, Adams DF, Nawfel RD, Zou KH, Judy PF (1999) CT fluoroscopy-guided abdominal interventions: techniques, results, and radiation exposure. *Radiology* 212:673–681
4. Wood BJ, Zhang H, Durrani A et al (2005) Navigation with electromagnetic tracking for interventional radiology procedures: a feasibility study. *J Vasc Interv Radiol* 16:493–505
5. Zaaroor M, Bejerano Y, Weinfeld Z, Ben-Haim S (2001) Novel magnetic technology for intraoperative intracranial frameless navigation: in vivo and in vitro results. *Neurosurgery* 48:1100–1107 discussion 1107–1108
6. Nagel M, Hoheisel M, Petzold R, Kalender WA, Krause UHW (2007) Needle and catheter navigation with electromagnetic tracking for computer-assisted C-arm CT interventions. *Proc SPIE* 6509:65090J.
7. Krucker J, Xu S, Glossop N et al (2007) Electromagnetic tracking for thermal ablation and biopsy guidance: clinical evaluation of spatial accuracy. *J Vasc Interv Radiol* 18:1141–1150
8. Froelich JJ, El-Sheik M, Wagner HJ, Achenbach S, Scherf C, Klose KJ (2000) Feasibility of C-arm-supported CT fluoroscopy in percutaneous abscess drainage procedures. *Cardiovasc Intervent Radiol* 23:423–430
9. Racadio JM, Babic D, Homan R et al (2007) Live 3D guidance in the interventional radiology suite. *AJR Am J Roentgenol* 189:W357–364
10. Akpek S, Brunner T, Benndorf G, Strother C (2005) Three-dimensional imaging and cone beam volume CT in C-arm angiography with flat panel detector. *Diagn Interv Radiol* 11:10–13
11. Krombach GA, Mahnken A, Tacke J et al (2001) US-guided nephrostomy with the aid of a magnetic field-based navigation device in the porcine pelvic caliceal system. *J Vasc Interv Radiol* 12:623–628
12. Holzknecht N, Helmberger T, Schoepf UJ et al (2001) Evaluation of an electromagnetic virtual target system (CT-guide) for CT-guided interventions. *Rofo* 173:612–618
13. Giraud P, Reboul F, Clippe S et al (2003) Respiration-gated radiotherapy: current techniques and potential benefits. *Cancer Radiother* 7(Suppl 1):15s–25s
14. Goerres GW, Burger C, Schwitter MR, Heidelberg TN, Seifert B, von Schulthess GK (2003) PET/CT of the abdomen: optimizing the patient breathing pattern. *Eur Radiol* 13:734–739
15. Herline A, Stefansic JD, Debelak J, Galloway RL, Chapman WC (2000) Technical advances toward interactive image-guided laparoscopic surgery. *Surg Endosc* 14:675–679
16. Nehmeh SA, Erdi YE, Pan T et al (2004) Quantitation of respiratory motion during 4D-PET/CT acquisition. *Med Phys* 31:1333–1338
17. Shimizu S, Shirato H, Aoyama H et al (2000) High-speed magnetic resonance imaging for four-dimensional treatment planning of conformal radiotherapy of moving body tumors. *Int J Radiat Oncol Biol Phys* 48:471–474
18. Azar FS, Metaxas DN, Schnall MD (2002) Methods for modeling and predicting mechanical deformations of the breast under external perturbations. *Med Image Anal* 6:1–27
19. Clifford MA, Banovac F, Levy E, Cleary K (2002) Assessment of hepatic motion secondary to respiration for computer assisted interventions. *Comput Aided Surg* 7:291–299
20. Solomon SB, Dickfeld T, Calkins H (2003) Real-time cardiac catheter navigation on three-dimensional CT images. *J Interv Card Electrophysiol* 8:27–36
21. Solomon SB, Magee C, Acker DE, Venbrux AC (1999) TIPS placement in swine, guided by electromagnetic real-time needle tip localization displayed on previously acquired 3-D CT. *Cardiovasc Intervent Radiol* 22:411–414
22. Solomon SB, Magee CA, Acker DE, Venbrux AC (1999) Experimental non-fluoroscopic placement of inferior vena cava filters: use of an electromagnetic navigation system with previous CT data. *J Vasc Interv Radiol* 10:92–95
23. Solomon SB, White P Jr, Wiener CM, Orens JB, Wang KP (2000) Three-dimensional CT-guided bronchoscopy with a real-time electromagnetic position sensor: a comparison of two image registration methods. *Chest* 118:1783–1787